

Two-color QCD at imaginary chemical potential and its impact on real chemical potential

Kouji Kashiwa,¹ Takahiro Sasaki,² Hiroaki Kouno,³ and Masanobu Yahiro²

¹*RIKEN/BNL Research Center, Brookhaven National Laboratory, Upton, NY-11973, USA*

²*Department of Physics, Graduate School of Sciences, Kyushu University, Fukuoka 812-8581, Japan*

³*Department of Physics, Saga University, Saga 840-8502, Japan*

(Dated: October 17, 2018)

We study properties of two-color QCD at imaginary chemical potential (μ) from the viewpoint of the Roberge-Weiss (RW) periodicity, the charge conjugation and the pseudo-reality. At $\mu = \pm i\pi T/2$, where T is temperature, the system is symmetric under the combination of the charge conjugation \mathcal{C} and the \mathbb{Z}_2 transformation. The symmetry, called $\mathcal{C}\mathbb{Z}_2$ symmetry, is preserved at lower T but spontaneously broken at higher T . The Polyakov-loop extended Nambu–Jona-Lasinio (PNJL) model has the same properties as two-color QCD for $\mathcal{C}\mathbb{Z}_2$ symmetry and the pseudo-reality. The nontrivial correlation between the chiral restoration and the deconfinement are investigated by introducing the entanglement vertex in the PNJL model. The order of $\mathcal{C}\mathbb{Z}_2$ symmetry breaking at the RW endpoint is second-order when the correlation is weak, but becomes first-order when the correlation is strong. We also investigate the impact of the correlation on the phase diagram at real μ .

PACS numbers: 11.30.Rd, 12.40.-y, 21.65.Qr, 25.75.Nq

I. INTRODUCTION

Elucidation of QCD at finite temperature (T) and finite quark-number chemical potential (μ) is one of the most important subjects in hadron physics. Lattice QCD (LQCD) is the first-principle calculation, but has the sign problem at real μ . Particularly at $\mu/T \gtrsim 1$, the LQCD calculation is not feasible, although several methods have been proposed so far to circumvent the problem; see for example Ref. [1]. For this reason, effective models such as the Polyakov-loop extended Nambu–Jona-Lasinio (PNJL) model [2–6] are widely used to investigate QCD at finite μ .

Symmetries are important to understand QCD. In this paper we focus our discussion on global symmetries. QCD has chiral symmetry in the limit of zero current quark mass (m) and \mathbb{Z}_{N_c} symmetry in the limit of infinite m , where N_c is the number of colors. Charge conjugation (\mathcal{C}) symmetry is preserved at $\mu = 0$ but not at finite μ , since the QCD action $S(\mu/T, T)$ is transformed by \mathcal{C} as

$$S(\mu/T, T) \xrightarrow{\mathcal{C}} S(-\mu/T, T). \quad (1)$$

This indicates that

$$Z(\mu/T, T) = Z^{(\mathcal{C})}(\mu/T, T) = Z(-\mu/T, T), \quad (2)$$

where $Z^{(\mathcal{C})}$ is the partition function written with the \mathcal{C} -transformed quark and gauge fields and the second equality comes from (1). Thus \mathcal{C} symmetry is broken at finite μ , but it derives the fact that $Z(\mu/T, T)$ is μ -even.

Similar discussion is possible also for imaginary chemical potential $\mu = i\theta T$, where θ is the dimensionless imaginary chemical potential. For simplicity, we use $S(\theta)$ and $Z(\theta)$ as shorthand notations of $S(i\theta, T)$ and $Z(i\theta, T)$, respectively. Consider the transformation

$$q(x, \tau) \rightarrow \exp(i\theta T\tau)q(x, \tau) \quad (3)$$

for the quark field q , where \mathbf{x} and τ are the spatial and imaginary time variables. After this transformation, the action $S(\theta)$ with the standard boundary condition $q(x, \beta) = -q(x, 0)$ is changed into $S(0)$ with the twisted boundary condition (TBC)

$$q(x, \beta) = -R(\theta)q(x, 0) \quad (4)$$

with the twist factor

$$R(\theta) = \exp(-i\theta). \quad (5)$$

The action $S(0)$ with the twist factor (5) in its quark boundary condition is a good starting point to understand roles of \mathcal{C} and \mathbb{Z}_{N_c} at finite θ . For example, one can easily see from (5) that $Z(\theta)$ has a periodicity of 2π . We can then consider one period of either $0 \leq \theta < 2\pi$ or $-\pi \leq \theta < \pi$.

The action $S(0)$ is not transformed by \mathcal{C} , but the twist factor is changed as

$$R(\theta) \xrightarrow{\mathcal{C}} R(-\theta). \quad (6)$$

This indicates that

$$Z(\theta) = Z^{(\mathcal{C})}(\theta) = Z(-\theta). \quad (7)$$

The action $S(0)$ is also invariant under the \mathbb{Z}_{N_c} transformation

$$q \rightarrow Uq, \quad A_\nu \rightarrow UA_\nu U^{-1} - i(\partial_\nu U)U^{-1}, \quad (8)$$

where A_ν is the gauge field and $U(x, \tau)$ are elements of $SU(N_c)$ with the boundary condition $U(x, \beta = 1/T) = \exp(-2i\pi k/N_c)U(x, 0)$ for integers $k = 0, \dots, N_c - 1$. However the \mathbb{Z}_{N_c} transformation changes $R(\theta)$ as [7]

$$R(\theta) \xrightarrow{\mathbb{Z}_{N_c}} R(\theta - 2\pi k/N_c). \quad (9)$$

This indicates that

$$Z(\theta) = Z^{(z)}(\theta) = Z(\theta - 2\pi k/N_c), \quad (10)$$

or equivalently

$$Z(\theta) = Z(\theta + 2\pi k/N_c), \quad (11)$$

where $Z^{(z)}$ is the partition function written with the \mathbb{Z}_{N_c} -transformed quark and gauge fields. Either (10) or (11) is called the Roberge-Weiss (RW) periodicity [7]. The periodicity means that $Z(\theta)$ is invariant under the combination of the \mathbb{Z}_{N_c} transformation and the parameter transformation $\theta \rightarrow \theta + 2\pi k/N_c$, i.e., under the extended \mathbb{Z}_{N_c} transformation [4].

At imaginary chemical potential, the \mathcal{C} and \mathbb{Z}_{N_c} thus break down through the quark boundary condition. As shown below, however, $R(\theta)$ is invariant under the \mathcal{C} transformation or the combination of the \mathcal{C} and \mathbb{Z}_{N_c} transformations at special values of θ . At $\theta = \pi$, $R(\theta)$ is \mathcal{C} -invariant, since $R(\pi) = R(-\pi)$. At $\theta = \pi/N_c$, $R(\theta)$ is invariant under the combination of the \mathcal{C} transformation and the \mathbb{Z}_{N_c} transformation with $k = -1$:

$$R(\pi/N_c) \xrightarrow{\mathcal{C}} R(-\pi/N_c) \xrightarrow{\mathbb{Z}_{N_c}} R(\pi/N_c). \quad (12)$$

QCD has the same symmetry at $\theta = \pi/N_c \bmod 2\pi/N_c$ because of the RW periodicity. We refer to this symmetry as $\mathcal{C}\mathbb{Z}_{N_c}$ symmetry in this paper, particularly when the \mathbb{Z}_{N_c} transformation used is not the identity transformation. An order parameter of the symmetry is a \mathcal{C} -odd and \mathbb{Z}_{N_c} -invariant quantity such as the quark number density n_q . In this sense $\mathcal{C}\mathbb{Z}_{N_c}$ symmetry has properties similar to \mathcal{C} symmetry.

For $N_c = 3$ as a typical case of odd N_c , there appears $\mathcal{C}\mathbb{Z}_3$ symmetry at $\theta = \pm\pi/3, \pi$. Particularly at $\theta = \pi$, the symmetry is reduced to \mathcal{C} symmetry. $\mathcal{C}\mathbb{Z}_3$ symmetries at $\theta = \pm\pi/3$ can be understood as \mathbb{Z}_3 images of \mathcal{C} symmetry at $\theta = \pi$. The symmetries at $\theta = 0, \pm\pi/3, \pi$ are summarized in Table I. Note that these symmetries may be spontaneously broken in some cases as shown below. Also for $N_c = 2$ as a typical case of even N_c , the system has $\mathcal{C}\mathbb{Z}_2$ symmetry at $\theta = \pm\pi/2$ and \mathcal{C} symmetry at $\theta = 0, \pi$; see Table II for the summary of symmetries. $\mathcal{C}\mathbb{Z}_2$ symmetries at $\theta = \pm\pi/2$ are, however, not \mathbb{Z}_2 images of \mathcal{C} symmetries at $\theta = 0, \pi$ because the number of \mathbb{Z}_2 images are 2. Further understanding is thus necessary for $\mathcal{C}\mathbb{Z}_{N_c}$ symmetry with even N_c .

When T is higher than some temperature T_{RW}^c , there appears a first-order phase transition at $\theta = \pi/N_c \bmod 2\pi/N_c$ [7]. Just on the transition line, the spontaneous breaking of either \mathcal{C} or $\mathcal{C}\mathbb{Z}_{N_c}$ symmetry takes place [8]. The transition is now called the RW phase transition. A current topic on the RW phase transition is the order of the transition at its endpoint, i.e., the RW endpoint. Recent three-color LQCD simulations show that the order is first-order for small and large m , but second-order for intermediate m [9–12]. The order may be first-order for both two-flavor [9, 10] and three-flavor cases [11, 12],

θ	\mathbb{Z}_3	\mathcal{C}	$\mathcal{C}\mathbb{Z}_3$
0	Invariant		
$\pm\pi/3$	Invariant		
π	Invariant		

TABLE I: Invariances of twist factor $R(\theta)$ in three-color QCD. $\mathcal{C}\mathbb{Z}_3$ transformation is defined with $k = \mp 1$ for $\theta = \pm\pi/3$. Note that $S(0)$ is invariant under both \mathbb{Z}_3 and \mathcal{C} transformations.

θ	\mathbb{Z}_2	\mathcal{C}	$\mathcal{C}\mathbb{Z}_2$
0, π	Invariant		
$\pm\pi/2$	Invariant		

TABLE II: Invariances of twist factor $R(\theta)$ in two-color QCD. $\mathcal{C}\mathbb{Z}_2$ transformation is defined with $k = \mp 1$ for $\theta = \pm\pi/2$. Note that $S(0)$ is invariant under both \mathbb{Z}_2 and \mathcal{C} transformations.

when the pion mass m_π has the physical value. If the order is first-order, the RW endpoint becomes a triple-point at which three first-order transition lines meet. The PNJL model reproduces these results [13–15].

Two-color QCD has some interesting points. The number of colors, N_c , can vary from 2 to infinity, that is, realistic three-color QCD is between two-color QCD and large N_c QCD. In this sense, understanding of both two-color and large- N_c QCD is important. The algebraic approach based on the pseudo-reality [16] plays an important role in two-color QCD, while large- N_c QCD is well understood by the geometric approach based on the $1/N_c$ expansion [17] or the AdS/CFT correspondence [18]. In virtue of the pseudo-reality, two-color LQCD has no sign problem not only at imaginary μ but also at real μ [19], and consequently LQCD data are available there [20–25]. Furthermore, two-color QCD has higher symmetry at imaginary μ than at real μ , that is $\mathcal{C}\mathbb{Z}_2$ symmetry at $\theta = \pm\pi/2$.

In this paper, we study properties of two-color QCD at imaginary μ from the viewpoint of the RW periodicity, $\mathcal{C}\mathbb{Z}_2$ symmetry and the pseudo-reality. The PNJL model has the same properties as two-color QCD for the RW periodicity, $\mathcal{C}\mathbb{Z}_2$ symmetry and the pseudo-reality. The PNJL model is then used to investigate two-color QCD concretely. Particularly, the nontrivial correlation between chiral and $\mathcal{C}\mathbb{Z}_2$ symmetry breakings are investigated.

This paper is organized as follows. In Sec. II, some properties of two-color QCD are derived with the \mathbb{Z}_2 transformation, the charge conjugation and the pseudo-reality. In Sec. III, the two-color PNJL model is formulated with the mean-field approximation. Numerical

results are shown in Sec. IV. Section V is devoted to summary.

II. PROPERTIES OF TWO-COLOR QCD

We first consider the one-flavor ($N_f = 1$) case. The partition function Z of two-color QCD is obtained in Euclidean spacetime as

$$Z = \int DA \det[M(\mu)] \exp\left[-\frac{1}{4g^2} F_{\mu\nu}^2\right] \quad (13)$$

with

$$M(\mu) = D + m - \gamma_4 \mu, \quad (14)$$

where the Dirac operator D is defined by $D = \gamma_\mu(\partial_\mu - iA_\mu)$ for the current quark mass m and the gauge field A_ν , and $F_{\mu\nu} = \partial_\mu A_\nu - \partial_\nu A_\mu - i[A_\mu, A_\nu]$. It is assumed that μ is either real or pure imaginary. For later convenience, we define Pauli matrices t_i in color space and the Dirac charge-conjugation matrix $C = \gamma_2 \gamma_4$.

The fermion determinant $\det[M(\mu)]$ satisfies

$$(\det[M(\mu)])^* = \det[M(-\mu^*)], \quad (15)$$

since

$$\begin{aligned} (\det[M(\mu)])^* &= \det[M(\mu)^\dagger] = \det[\gamma_5 M(\mu)^\dagger \gamma_5] \\ &= \det[M(-\mu^*)]. \end{aligned} \quad (16)$$

The relation (15) indicates that $\det[M(\mu)]$ is real when μ is pure imaginary. The relation (15) is true for any N_c .

Two-color QCD has the pseudo-reality [16],

$$Dt_2 C \gamma_5 = t_2 C \gamma_5 D^*, \quad (17)$$

and hence the fermion determinant satisfies

$$\begin{aligned} \det[M(\mu)] &= \det[(t_2 C \gamma_5)^{-1} M(\mu) (t_2 C \gamma_5)] \\ &= (\det[M(\mu^*)])^* \end{aligned} \quad (18)$$

in virtue of the pseudo-reality (17). This means that $\det[M(\mu)]$ is real when μ is real. Two-color LQCD thus has no sign problem at both real and pure imaginary μ [19]. The charge-conjugation relation (2) is obtained from (15) and (18).

The Polyakov loop Φ is the vacuum expectation value of the Polyakov-loop operator

$$L = \frac{1}{N_c} \text{tr}_c \left(\mathcal{P} \exp \left[i \int_0^{1/T} d\tau A_4 \right] \right). \quad (19)$$

with the time-ordering operator \mathcal{P} . The operator L is real in the two-color system, because

$$L^* = \frac{1}{2} \text{tr}_c \left(\mathcal{P} \exp \left[-i \int_0^{1/T} d\tau (A_4)^* \right] \right) = L, \quad (20)$$

where the second equality is obtained from the identity $t_2 A_\nu t_2 = -(A_\nu)^T = -(A_\nu)^*$. The Polyakov loop Φ is hence real at both real and pure imaginary μ ; note that $\det[M(\mu)]$ is real there. Under the charge conjugation, the factor $-(A_4)^T$ is transformed into A_4 . Therefore the second equality of (20) means that L is \mathcal{C} -invariant. Using this property and the relation (2), one can see that

$$\Phi(\mu/T, T) = \Phi(-\mu/T, T). \quad (21)$$

For pure imaginary chemical potential $\mu = iT\theta$, it is convenient to introduce the modified Polyakov loop

$$\Psi(\theta) \equiv \Phi(\theta) e^{i\theta}, \quad (22)$$

where $\Phi(\theta)$ has been used as a shorthand notation of $\Phi(i\theta, T)$. The modified Polyakov loop satisfies the RW periodicity

$$\Psi(\theta) = \Psi(\theta + \pi), \quad (23)$$

since it is invariant under the extended \mathbb{Z}_{N_c} transformation [4]. Inserting (22) into (23) leads to

$$\Phi(\theta) = -\Phi(\theta + \pi). \quad (24)$$

One can also see from (21), (22) and $\Phi^*(\theta) = \Phi(\theta)$ that

$$\Phi(\theta) = \Phi(-\theta), \quad \Psi(\theta)^* = \Psi(-\theta). \quad (25)$$

Hence the imaginary part $\text{Im}[\Psi(\theta)]$ is θ -odd, whereas the real part $\text{Re}[\Psi(\theta)]$ and $\Phi(\theta)$ are θ -even.

At $\theta = \pm\pi/2$, two-color QCD has $\mathcal{C}\mathbb{Z}_2$ symmetry, as mentioned in Sec. I. And $\Phi(\theta)$ and $\text{Im}[\Psi(\theta)]$ are order parameters of the symmetry, since $\Phi(\theta)$ and $\text{Im}[\Psi(\theta)]$ are $\mathcal{C}\mathbb{Z}_2$ -odd at $\theta = \pm\pi/2$:

$$\Phi(\theta) \xrightarrow{\mathcal{C}} \Phi(-\theta) \xrightarrow{\mathbb{Z}_2} -\Phi(\theta), \quad (26)$$

$$\text{Im}[\Psi(\theta)] \xrightarrow{\mathcal{C}} \text{Im}[\Psi(-\theta)] \xrightarrow{\mathbb{Z}_2} -\text{Im}[\Psi(\theta)], \quad (27)$$

because L is \mathcal{C} -invariant and transformed by the \mathbb{Z}_2 transformation as $L \rightarrow -L$. The two order parameters are identical with each other at $\theta = \pm\pi/2$, since $\text{Im}[\Psi(\theta)] = \Phi(\theta) \sin(\theta) = \Phi(\theta)$. This is not surprising, because two-color QCD has only one symmetry there. At $\theta = 0, \pi$, meanwhile, QCD has \mathcal{C} symmetry and the order parameter is a \mathcal{C} -odd quantity such as n_q . Table II shows the symmetries that two-color QCD has at $\theta = 0, \pm\pi/2, \pi$.

Next we consider the $N_f = 2$ case. The fermion determinant is described by

$$\det[M(\mu)] = \det[M_u(\mu)] \det[M_d(\mu)], \quad (28)$$

where $\det[M_u(\mu)]$ and $\det[M_d(\mu)]$ are the fermion determinants for u- and d-quark, respectively. Using the operator Ct_2 only for $\det[M_d(\mu)]$, one can get the relation

$$\begin{aligned} \det[M(\mu)] &= \det[M_u(\mu)] \det[(Ct_2)^{-1} M_d(\mu) (Ct_2)] \\ &= \det[M_u(\mu)] \det[M_d(-\mu)]. \end{aligned} \quad (29)$$

This relation indicates that the 1+1 system with finite μ is identical with the 1+1* system with the same amount of isospin chemical potential μ_{iso} . The diquark condensate in the former system corresponds to the pion condensate in the latter system. Because of this symmetry, we consider the former system only in the present paper.

Two-color LQCD simulations were made in Ref. [20, 21, 23, 25] for the $N_f = 8$ case. The LQCD results at $\theta = \pi/2$ show that $\Phi = 0$ at small T but finite at large T . This indicates that the spontaneous breaking of $\mathcal{C}\mathbb{Z}_2$ symmetry occurs at some temperature T_{RW}^c . Further analyses are made in Sec. III and IV by using the PNJL model.

III. PNJL MODEL

We consider the $N_c = N_f = 2$ case. The PNJL Lagrangian is obtained in Minkowski spacetime by

$$\begin{aligned} \mathcal{L} = & \bar{q}(i\gamma^\nu D_\nu - m)q \\ & + G[(\bar{q}q)^2 + (\bar{q}i\gamma_5\vec{\tau}q)^2 + |q^T Ci\gamma_5\tau_2 t_2 q|^2] \\ & - G_v(\bar{q}\gamma^\mu q)^2 - \mathcal{U}(\Phi), \end{aligned} \quad (30)$$

where q is the two-flavor quark field, m is the current quark mass and t_i and τ_i are Pauli matrices in color and flavor spaces, respectively. In the limit of $m = \mu = 0$, two-color QCD has Pauli-Gürsey symmetry [26, 27], so the PNJL Lagrangian is so constructed as to have the symmetry. Note that the vector-type four-quark interaction $(\bar{q}\gamma^\mu q)^2$ does not work at $\mu = 0$ in the mean-field level, since the vector-type condensate is zero at $\mu = 0$. The potential \mathcal{U} is a function of the Polyakov loop Φ and the explicit form is shown later in Sec. IV.

Using the mean-field approximation, one can get the effective potential Ω as [28]

$$\begin{aligned} \Omega = & -2N_f \int \frac{d^3p}{(2\pi)^3} \sum_{\pm} \left[\frac{1}{2} N_c E_p^\pm + T(\ln f^- + \ln f^+) \right] \\ & + U + \mathcal{U}(\Phi) \end{aligned} \quad (31)$$

with

$$f^\pm = 1 + 2\Phi e^{-\beta E_p^\pm} + e^{-2\beta E_p^\pm}, \quad (32)$$

$$U = G(\sigma^2 + \Delta^2) - G_v n_q^2 \quad (33)$$

for the chiral condensate $\sigma = \langle \bar{q}q \rangle$, the diquark condensate $\Delta = |\langle q^T Ci\gamma_5\tau_2 t_2 q \rangle|$ and the vector condensate (quark number density) $n_q = \langle q^\dagger q \rangle$. Here the factors E_p^\pm are defined by

$$E_p^\pm = \text{sgn}(E_p \pm \mu_v) \sqrt{(E_p \pm \mu_v)^2 + (2G\Delta)^2}, \quad (34)$$

for finite Δ and

$$E_p^\pm = E_p \pm \mu_v \quad (35)$$

for $\Delta = 0$, where $\text{sgn}(E_p \pm \mu_v)$ is the sign function, $E_p = \sqrt{p^2 + M^2}$, $M = m - 2G\sigma$ and $\mu_v = \mu - 2G_v n_q$. In the limit of $m = \mu = 0$, the condensate n_q is zero, so that Ω becomes invariant under the rotation in the σ - Δ plane as a consequence of Pauli-Gürsey symmetry.

In the Polyakov gauge, the Polyakov-loop Φ is obtained by

$$\Phi = \frac{1}{2} (e^{i\phi} + e^{-i\phi}) = \cos(\phi) \quad (36)$$

for real number ϕ , indicating that Φ is real. The mean fields $X = \sigma, \Delta, n_q, \Phi$ are determined from the stationary conditions

$$\frac{\partial \Omega}{\partial X} = 0, \quad (37)$$

where Ω is regularized by the three-dimensional momentum cutoff

$$\int \frac{d^3p}{(2\pi)^3} \rightarrow \frac{1}{2\pi^2} \int_0^\Lambda dp p^2, \quad (38)$$

because this model is nonrenormalizable.

At imaginary chemical potential $\mu = i\theta T$, Ω is invariant under the extended \mathbb{Z}_2 transformation [4]

$$\Phi \rightarrow e^{-i\pi} \Phi, \quad \theta \rightarrow \theta + \pi. \quad (39)$$

This can be understood easily by introducing the modified Polyakov-loop $\Psi = e^{i\theta} \Phi$ and its conjugate $\Psi^* = e^{-i\theta} \Phi$ invariant under the extended \mathbb{Z}_2 transformation. The condensate Δ is zero at imaginary μ , since Δ becomes finite only for $\mu^2 \geq m_\pi^2/4$ [13, 16]. When $\Delta = 0$, Ω is rewritten into the form of (31) with

$$f^+ = 1 + 2\Psi e^{-2i\theta} e^{-\beta(E_p - 2G_v n_q)} + e^{-2\beta E_p^+}, \quad (40)$$

$$f^- = 1 + 2\Psi^* e^{2i\theta} e^{-\beta(E_p + 2G_v n_q)} + e^{-2\beta E_p^-}. \quad (41)$$

Obviously, Eqs. (40) and (41) show that Ω is invariant under the extended \mathbb{Z}_2 transformation and at the same time that Ω has a periodicity of π in θ , i.e., the RW periodicity

$$\Omega(\theta) = \Omega(\theta + \pi). \quad (42)$$

It should be noted that if Δ is finite, Ω will not have the RW periodicity. Since θ -dependence of mean fields $X = \sigma, n_q, \Psi$ are determined from Ω by the stationary conditions (37), all the X have the RW periodicity

$$X(\theta) = X(\theta + \pi). \quad (43)$$

Furthermore, the RW periodicity $\Psi(\theta) = \Psi(\theta + \pi)$ yields the relation

$$\Phi(\theta) = -\Phi(\theta + \pi). \quad (44)$$

The PNJL Lagrangian \mathcal{L} is invariant under the combination of the \mathcal{C} and the parameter transformation

$\theta \rightarrow -\theta$. This property guarantees that $\Omega(\theta) = \Omega(-\theta)$ and thereby \mathcal{C} -even quantities σ , Δ and Φ are θ -even, whereas \mathcal{C} -odd quantity n_q is θ -odd. In the PNJL Lagrangian, θ appears only through the pure imaginary factor $i\theta$. This shows that θ -odd quantities become pure imaginary, while θ -even quantities become real. The second equation of (25) is obtainable from the fact that $\Phi(\theta)^* = \Phi(\theta) = \Phi(-\theta)$, namely

$$\Psi(\theta)^* = (\Phi(\theta)e^{i\theta})^* = \Phi(\theta)^* e^{-i\theta} = \Psi(-\theta). \quad (45)$$

The PNJL model thus has the same properties as two-color QCD for the RW periodicity and the θ -parity.

Using (44) and $\Phi(\theta) = \Phi(-\theta)$, one can see that

$$\Phi(\theta) = -\Phi(\pi - \theta) \quad (46)$$

and hence $\Phi(\theta) = 0$ at $\theta = \pi/2$, if Φ is a smooth function of θ . When T is larger than some temperature T_{RW} , Ω is not a smooth function of θ at $\theta = \pi/2$. This is the RW phase transition. Once the RW phase transition occurs, $\Phi(\theta)$ is not smooth at $\theta = \pi/2$ and consequently $\Phi(\theta)$ becomes finite there. This means that the spontaneous breaking of \mathcal{CZ}_2 symmetry takes place on the RW phase transition line.

The relations (43) and (45), meanwhile, yield a similar relation to (46):

$$\text{Im}[\Psi(\theta)] = -\text{Im}[\Psi(\pi - \theta)] \quad (47)$$

At $\theta = \pm\pi/2$, therefore, $\text{Im}[\Psi]$ serves as an order parameter of \mathcal{CZ}_2 symmetry as well as Φ .

IV. NUMERICAL RESULTS

A. Parameter setting

For the $N_c = N_f = 2$ case, we do not have enough LQCD data at imaginary chemical potential. We then make qualitative analyses here. It is well known from the nonlocal version of the PNJL model [5, 6, 29–33] that there is the correlation between the chiral order-parameter and the Polyakov-loop in the coupling constant through the distribution function. This feature can be phenomenologically introduced in the local PNJL model by using the entanglement vertex [14]. This entanglement is taken into account in the present analysis. We make the following parameter setting.

1. Since the ratio $r \equiv G_v/G$ is of order $(N_c)^0$ in the leading order of the $1/N_c$ expansion, we take $r = 0.4$ that is determined from the $N_c = 3$ case by comparing the result of the nonlocal PNJL model with LQCD data at finite imaginary chemical potential.
2. We introduce the entanglement vertex of the form $G_i(1 - \alpha\Phi^2)$ for $G_i = G$ and G_v , respecting \mathbb{Z}_2 symmetry. Here the entanglement parameter α is

treated as a free parameter, but is assumed to be common for both G and G_v . Vacuum properties are unchanged for any value of α . We mainly use $\alpha = 0.4$ at which pseudo-critical temperatures of the chiral and deconfinement transitions almost coincide when $\mu = 0$.

3. In the leading order of the $1/N_c$ expansion, m_π is scaled by $(N_c)^0$ and the pion decay constant f_π by $\sqrt{N_c}$. These scaling properties are assumed to determine the parameter set (G, Λ, m) of the NJL sector, where m is simply assumed to be 5.4 MeV. In this parameter set, the dynamical quark mass M becomes $M_0 = 305$ MeV at $T = \mu = 0$. The resulting parameters are shown in Table III, together with the values of m_π , f_π and M_0 .
4. Following Ref. [28], we take the Polyakov-loop effective potential of the form

$$\frac{\mathcal{U}(\Phi)}{T} = -b \left[24e^{-a/T}\Phi^2 + \ln(1 - \Phi^2) \right] \quad (48)$$

with $a = 858.1$ MeV and $b^{1/3} = 210.5$ MeV. This potential yields a second-order deconfinement transition in the pure gauge limit.

In Ref. [34], the scalar coupling G was varied to investigate the effect on the phase transition. In this case, however, the change of G also varies vacuum properties such as m_π and f_π . We therefore fix G in this paper not to change the vacuum properties. The Polyakov-loop effective potential \mathcal{U} used here is determined by using the strong coupling expansion of the pure Yang-Mills theory. The logarithmic part comes from the Haar measure. Since the parameter fitting procedure does not refer to microscopic dynamics, it is unclear how the Polyakov-loop effective potential is related to non-perturbative characteristics near T_c . This problem should be investigated elsewhere by considering other approach based on gluon and ghost propagators [35].

m_π [MeV]	f_π [MeV]	M_0 [MeV]
140	75.4	305
G [GeV ⁻²]	Λ [MeV]	m [MeV]
7.23	657	5.4

TABLE III: Summary of parameters and physical values.

B. θ dependence of order parameters

Figures 1(a)-(c) represent θ dependence of M , $\text{Im}[\Psi]$ and Φ , respectively, for three cases of $\alpha = 0, 0.2$ and 0.4 . Here we consider a high- T case of $T = 2.5m_\pi$. M is

an order parameter of chiral symmetry, while $\text{Im}[\Psi]$ and Φ are order parameters of \mathcal{CZ}_2 symmetry, respectively. Equations (43)-(47) show that Φ is antisymmetric with respect to the $\theta = \pi/2$ axis, whereas M is symmetric with respect to the axis. In addition, $\text{Im}[\Psi]$ is antisymmetric with respect to the $\theta = \pi/2$ axis and zero at $\theta = 0$ and π . As shown in panel (b), $\text{Im}[\Psi]$ has a gap at $\theta = \pi/2$, indicating that \mathcal{CZ}_2 symmetry is spontaneously broken there for the high- T case. The zeroth-order discontinuity (gap) in $\text{Im}[\Psi]$ means that a first-order phase transition takes place at $\theta = \pi/2$. This is the RW phase transition [7]. At $\theta = \pi/2$, Φ also has a gap, since $\text{Im}[\Psi] = \Phi$ at $\theta = \pi/2$. This is a characteristic of two-color QCD.

The \mathcal{CZ}_2 -even quantity M has a cusp at $\theta = \pi/2$, when the \mathcal{CZ}_2 -odd quantities $\text{Im}[\Psi]$ and Φ have a gap there. In general, the zeroth-order discontinuity (gap) in a \mathcal{CZ}_2 -odd quantity is propagated to other \mathcal{CZ}_2 -odd quantities as the zeroth-order discontinuity (gap) and to \mathcal{CZ}_2 -even quantities as the first-order discontinuity (cusp) [36, 37]. The order parameters $\text{Im}[\Psi]$ and Φ are less sensitive to α than M .

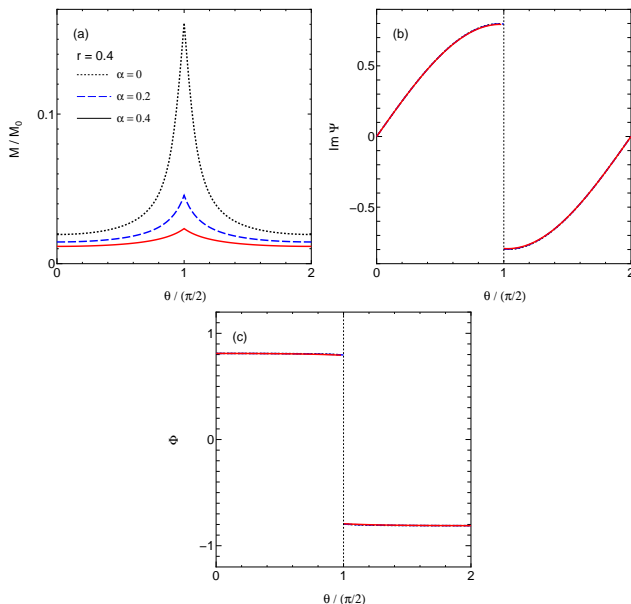


FIG. 1: θ -dependence of order parameters (a) M , (b) $\text{Im}[\Psi]$ and (c) Φ at $T = 2.5m_\pi$. Here M is normalized by the value M_0 at $T = \mu = 0$. The dotted, dashed and solid lines represent the results of $\alpha = 0, 0.2$ and 0.4 , respectively.

C. Interplay between chiral and deconfinement transitions

Figure 2 shows T -dependence of M/M_0 and $|\Phi|$ at $\theta = \pi/2$ for three cases of $\alpha = 0, 0.2$ and 0.4 . The \mathcal{CZ}_2 -symmetry breaking takes place at some temperature T_d^c , and the order is second-order for $\alpha = 0$ and 0.2 , but becomes first-order for $\alpha = 0.4$. Here the vertical thin-

dotted line denotes the critical temperature of the first-order transition. The chiral transition is crossover for $\alpha = 0$ and 0.2 , but it becomes first-order for $\alpha = 0.4$. The entanglement thus intensifies both the chiral transition and the \mathcal{CZ}_2 -symmetry breaking. For $\alpha = 0$ and 0.2 , M has a cusp at $T = T_d^c$ as a result of the propagation of the first-order discontinuity in $|\Phi|$ [37].

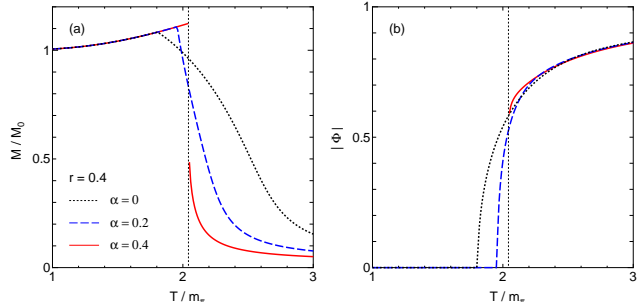


FIG. 2: T -dependence of (a) M/M_0 and (b) $|\Phi|$ at $\theta = \pi/2$. The dotted, dashed and solid lines represent the results of $\alpha = 0, 0.2$ and 0.4 , respectively.

Figure 3 shows T -dependence of M/M_0 and Φ at $\theta = 0$ ($\mu = 0$), where Φ is an order parameter of the deconfinement transition. Both the deconfinement and chiral transitions keep crossover for $\alpha = 0, 0.2$ and 0.4 , although the transitions become stronger as α increases. The pseudo-critical temperature T_d^c of the deconfinement transition is less sensitive to α than the pseudo-critical temperature T_χ^c of the chiral transition, where the pseudo-critical temperatures are defined by peak positions of dM/dT and $d\Phi/dT$, respectively.

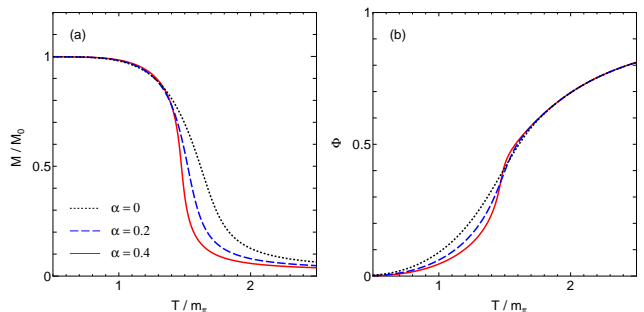


FIG. 3: T -dependence of (a) M/M_0 and (b) Φ at $\mu = 0$. See Fig. 2 for the definition of lines.

As shown in Fig 2, the \mathcal{CZ}_2 symmetry breaking takes place on a line of $\theta = \pi/2$ and $T \geq T_d^c$. As discussed in Sec. III, the line is the RW phase transition line; therefore, $T_d^c = T_{\text{RW}}^c$. This endpoint is called the RW endpoint. As shown later in Fig. 6, the spontaneous breaking of \mathcal{CZ}_2 symmetry at the RW endpoint is continuously connected to the deconfinement

transition at $0 \leq \theta < \pi/2$. Thus the crossover deconfinement transition at $\theta = 0$ is a remnant of the \mathcal{CZ}_2 symmetry breaking at the RW endpoint. Hence, for simplicity, we regard the \mathcal{CZ}_2 symmetry breaking at the RW endpoint as a part of the deconfinement transition at $0 \leq \theta < \pi/2$.

Dynamics at $\theta = \pi/2$ is more complicated than that at $\mu = 0$, since the order parameters have discontinuities of either the zeroth or the first order at $\theta = \pi/2$. The order parameters are considered to be more sensitive to α near the discontinuities. This is really true as seen by comparing Fig. 2 with Fig. 3. Through the discontinuities, we can then investigate clearly how strong the entanglement between the chiral and deconfinement transitions is. The symmetry breakings at $\theta = \pi/2$ thus give deeper understanding.

Figure 4 shows α -dependence of two (pseudo)critical temperatures T_d^c and T_χ^c at $\theta = \pi/2$ and 0. The two (pseudo)critical temperatures approach each other as α increases, and finally agree with each other at $\alpha \gtrsim 0.2$ for $\theta = \pi/2$ and at $\alpha \gtrsim 0.4$ for $\theta = 0$. As for $\alpha \lesssim 0.2$, the speed of the approach is much faster for $\theta = \pi/2$ than for $\theta = 0$. The entanglement thus makes it stronger the correlation between the chiral and deconfinement transitions. Therefore, the difference $|T_\chi^c - T_d^c|$ is a good quantity to determine the value of α . For $\theta = \pi/2$, the deconfinement transition is second-order at $\alpha < \alpha_c \approx 0.33$, but first-order at $\alpha > \alpha_c$. The chiral transition is, meanwhile, crossover at $\alpha < \alpha_c$, although it is first-order at $\alpha > \alpha_c$. Hence, the point at $\alpha = \alpha_c$ is a tri-critical point (TCP) for the deconfinement transition and a critical endpoint for the chiral transition.

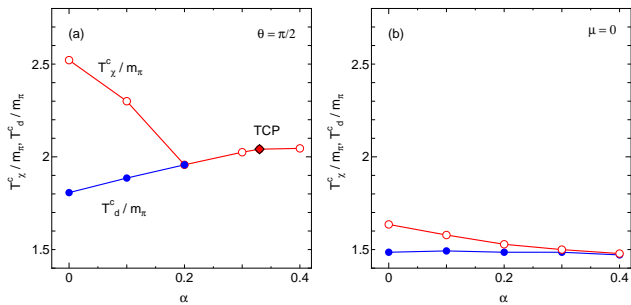


FIG. 4: α -dependence of (pseudo)critical temperatures T_d^c and T_χ^c at (a) $\theta = \pi/2$ and (b) $\mu = 0$ for the case of $G_v = 0.4G$. The close diamond symbol with “TCP/CEP” stands for the point that is a TCP for the deconfinement transition and a CEP for the chiral transition. The numerical values have ambiguities of about 1 MeV and the solid lines are drawn by connecting two neighborhood points.

Figure 5 shows r -dependence of M/M_0 and $|\text{Im } \Psi|$ at $\theta = \pi/2$. The effect of r is similar to that of α , but the former effect is smaller than the latter one, when r is varied within a realistic range from 0.25 to 0.5.

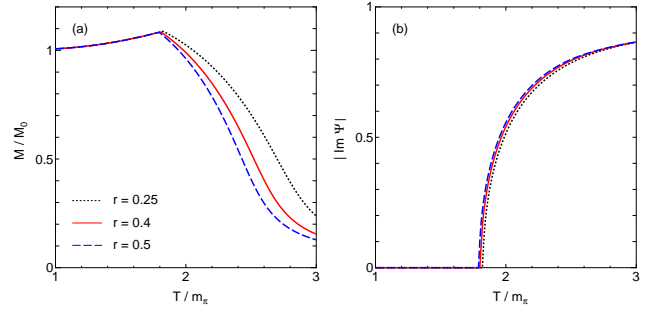


FIG. 5: T -dependence of (a) M/M_0 and (b) $|\text{Im } \Psi|$ at $\theta = \pi/2$. The dotted, dashed and solid lines denote the results for $r = 0.25, 0.4$ and 0.5 , respectively. Here α is set to 0.4 .

D. Phase diagram at imaginary and real chemical potentials

First we consider the phase diagram at imaginary μ for two cases of $\alpha = 0$ and 0.4 . Here we take $r = 0.4$. Figure 6 shows the phase diagram in the θ - T plane. In the left panel for the case of $\alpha = 0$, the upper and lower dotted lines denote chiral and deconfinement crossover transitions, respectively. The two transitions are thus separated from each other, when the correlation between the two transitions is weak. In this situation, the \mathcal{CZ}_2 symmetry breaking at the RW endpoint $(\theta, T) = (\pi/2, T_{RW}^c)$ is second-order. In the right panel for the strong correlation case of $\alpha = 0.4$, the two crossover transitions (dotted lines) agree with each other and the \mathcal{CZ}_2 symmetry breaking at the RW endpoint becomes first-order. In other words, the RW endpoint becomes a triple-point where three first-order transition lines meet. Thus, the RW endpoint becomes a triple-point, when the correlation between the chiral and deconfinement transition are strong.

The Polyakov-loop effective potential used in this study yields the second-order \mathbb{Z}_2 symmetry breaking in the heavy quark limit. Since the entanglement parameter α makes the symmetry breaking stronger, the first-order \mathcal{CZ}_2 symmetry breaking in the physical quark mass does not come from the \mathcal{CZ}_2 symmetry breaking only. The chiral transition becomes stronger, if the coupling constant G is weakened at finite T ; see for example Ref. [38]. In the present model, the coupling constant is weakened through the entanglement vertex, so that the chiral transition becomes first-order. This behavior is seen in the left panel of Fig. 2. The first-order \mathcal{CZ}_2 symmetry breaking is therefore induced by the first-order chiral transition.

Next we investigate an influence of α on the phase diagram at real μ . Figure 7 shows T -dependence of M/M_0 , Φ , Δ/σ_0 and n_q for the case of $r = 0.4$ and $\mu = m_\pi$, where σ_0 is the absolute value of σ at $T = \mu = 0$. As shown in panel (c), Δ/σ_0 vanishes around $T = 1.5m_\pi$, indicating that the superfluid/normal transition occurs

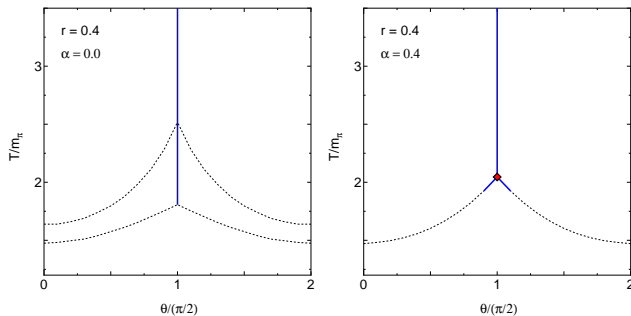


FIG. 6: The phase diagram in the θ - T plane for $\alpha = 0$ (left panel) and $\alpha = 0.4$ (right panel). Here the case of $r = 0.4$ is taken. The dotted and solid lines stand for crossover and first-order transitions, respectively. In the left panel, the upper and lower dotted lines mean the chiral and deconfinement crossover lines, respectively. In the right panel, the chiral and deconfinement crossover lines almost coincide with each other, and the diamond symbol denotes the triple-point.

there. The phase boundary is rather sensitive to α .

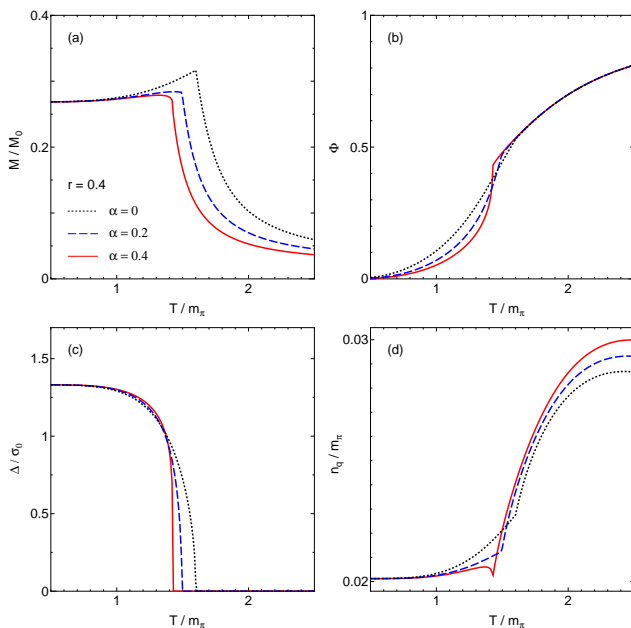


FIG. 7: T -dependence of (a) M/M_0 , (b) Φ , (c) Δ/σ_0 and (d) n_q for the case of $r = 0.4$ and $\mu = m_\pi$. The dotted and solid lines represent the results of $\alpha = 0$ and 0.4 , respectively.

In this study, we take $r \equiv G_v/G = 0.4$ for all the calculations. Although this value is obtained from the PNJL results with the corresponding LQCD data, it is not easy to determine the value definitely. We then check r -dependence of order parameters, as shown in Fig. 8 where $r = 0.25$ and 0.5 are taken as lower and upper limits of a reliable range of r . Effects of r on M , Φ and Δ are rather small, although

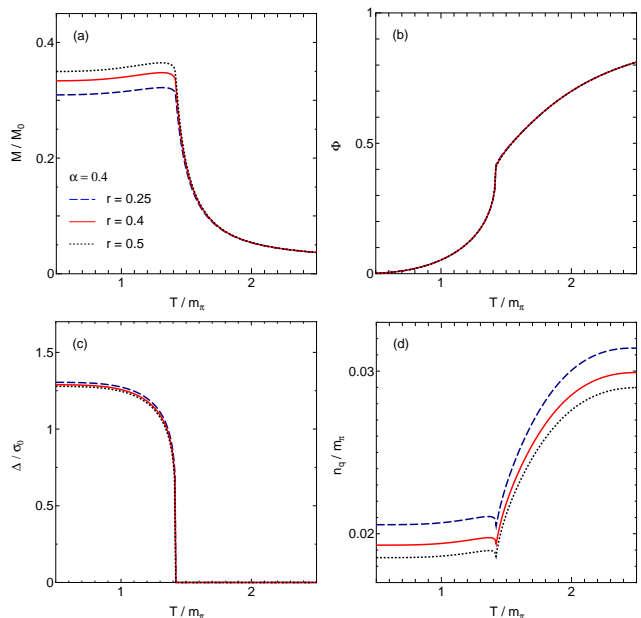


FIG. 8: T -dependence of (a) M/M_0 , (b) Φ , (c) Δ/σ_0 and (d) n_q for the case of $\alpha = 0.4$ and $\mu = m_\pi$. The dotted, solid and dashed lines represent the results of $r = 0.25$, 0.4 and 0.5 , respectively.

r gives an appreciable effect on n_q .

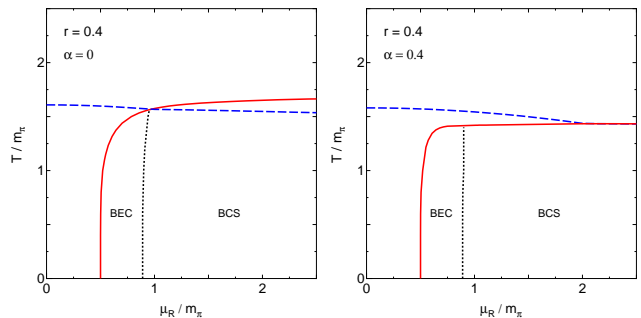


FIG. 9: The phase diagram in the μ - T plane for $\alpha = 0$ (left panel) and 0.4 (right panel). Here the case of $r = 0.4$ is taken. The dotted, dashed and solid lines stand for the BCS-BEC crossover ($M = \mu$), the deconfinement crossover ($\Phi = 0.5$) and the superfluid/normal transition lines, respectively.

Finally we consider the phase diagram at real μ . Figure 9 shows the BCS-BEC crossover ($M = \mu$), the deconfinement crossover ($\Phi = 0.5$) and the superfluid/normal transition lines for two cases of $\alpha = 0$ and 0.4 ; see Ref. [28] for the definitions of these transitions. When T is small, the superfluid/normal transition occurs at $\mu = m_\pi/2$ as expected. When $T > m_\pi$ and $\mu > m_\pi/2$, meanwhile, the superfluid/normal transition takes place around $T = 1.5m_\pi$. The transition line depends on α rather strongly compared with the BCS-BEC crossover and the deconfinement crossover line. Thus the correla-

tion between the chiral and deconfinement transitions is important not only at $\mu^2 = -(T\pi/2)^2$ but also at large real μ such as $\mu^2 > (m_\pi/2)^2$.

V. SUMMARY

We have studied properties of two-color QCD at imaginary $\mu = i\theta T$ from the viewpoint of the RW periodicity, the pseudo-reality and \mathcal{CZ}_2 symmetry. Two-color QCD has \mathcal{CZ}_2 symmetry at $\theta = \pm\pi/2$. The PNJL model has the same properties as two-color QCD for the RW periodicity, the pseudo-reality and \mathcal{CZ}_2 symmetry. The PNJL model is thus a good model to investigate two-color QCD at imaginary μ concretely. We have then investigated the nontrivial correlation between the deconfinement and chiral transitions at imaginary μ for the two-flavor case.

At $\theta = \pi/2$ and $T \geq T_{\text{RW}}^c$, i.e., on the RW phase-transition line, the spontaneous breaking of \mathcal{CZ}_2 symmetry takes place. The \mathcal{CZ}_2 symmetry breaking at the RW endpoint $(\theta, T) = (\pi/2, T_{\text{RW}}^c)$ is continuously connected to the deconfinement transition at $0 \leq \theta < \pi/2$. Thus the crossover deconfinement transition at $\theta = 0$ is a remnant of the \mathcal{CZ}_2 symmetry breaking at the RW endpoint.

The order of the \mathcal{CZ}_2 symmetry breaking at the RW endpoint is nontrivial. It cannot be determined by \mathcal{CZ}_2 symmetry and the pseudo-reality. The order depends on the strength of the entanglement parameter α , i.e., the strength of the correlation between chiral and \mathcal{CZ}_2 symmetry breakings. The order is second-order for small α ,

but becomes first-order for large α . The second-order nature is originated in the Polyakov-loop effective potential. Meanwhile, the first-order nature comes from the fact that chiral symmetry breaking becomes first-order as a consequence of the strong entanglement. The order of \mathcal{CZ}_2 symmetry breaking at the RW endpoint is thus sensitive to the strength of the correlation between chiral and \mathcal{CZ}_2 symmetry breakings. Finally, we have investigated the impact of α on the phase diagram at real μ . The diagram, particularly the superfluid transition, is rather sensitive to α . The determination of α is thus important for both real and imaginary μ .

At the present stage, we do not know how large α is, but it is possible to determine the value of α from LQCD simulations at $\theta = \pi/2$, particularly by seeing the correlation between chiral and \mathcal{CZ}_2 symmetry breakings. It is interesting as a future work. In two-color QCD, the correlation between the chiral and deconfinement transitions is thus important for both real and imaginary μ . This is true also for three-color QCD. This strongly suggests that understanding of three-color QCD at imaginary μ is important to determine the phase diagram at real μ .

Acknowledgments

K.K. is supported by RIKEN Special Postdoctoral Researchers Program. T.S. is supported by JSPS KAKENHI Grant Number 23-2790.

-
- [1] P. de Forcrand, PoS (LAT2009) p. 010 (2009), 1005.0539.
 - [2] K. Fukushima, Phys. Lett. **B591**, 277 (2004), hep-ph/0310121.
 - [3] C. Ratti, M. A. Thaler, and W. Weise, Phys. Rev. D **73**, 014019 (2006), hep-ph/0506234.
 - [4] Y. Sakai, K. Kashiwa, H. Kouno, and M. Yahiro, Phys. Rev. D **77**, 051901 (2008), 0801.0034.
 - [5] T. Hell, S. Roessner, M. Cristoforetti, and W. Weise, Phys. Rev. D **79**, 014022 (2009), 0810.1099.
 - [6] K. Kashiwa, T. Hell, and W. Weise, Phys. Rev. D **84**, 056010 (2011), 1106.5025.
 - [7] A. Roberge and N. Weiss, Nucl. Phys. **B275**, 734 (1986).
 - [8] H. Kouno, Y. Sakai, K. Kashiwa, and M. Yahiro, J. Phys. G **36**, 115010 (2009), 0904.0925.
 - [9] M. D'Elia and F. Sanfilippo, Phys. Rev. D **80**, 111501(R) (2009), 0909.0254.
 - [10] C. Bonati, G. Cossu, M. D'Elia, and F. Sanfilippo, Phys. Rev. D **83**, 054505 (2011), 1011.4515.
 - [11] P. de Forcrand and O. Philipsen, Phys. Rev. Lett. **105**, 152001 (2010), 1004.3144.
 - [12] C. Bonati, P. de Forcrand, M. D'Elia, O. Philipsen, and F. Sanfilippo (2012), 1201.2769.
 - [13] Y. Sakai, H. Kouno, and M. Yahiro, J. Phys. **G37**, 105007 (2010), 0908.3088.
 - [14] Y. Sakai, T. Sasaki, H. Kouno, and M. Yahiro, Phys. Rev. **D82**, 076003 (2010), 1006.3648.
 - [15] T. Sasaki, Y. Sakai, H. Kouno, and M. Yahiro, Phys. Rev. D **84**, 091901 (2011), 1105.3959.
 - [16] J. B. Kogut, M. A. Stephanov, D. Toublan, J. J. M. Verbaarschot, and A. Zhitnitsky, Nucl. Phys. **B582**, 477 (2000), hep-lat/0001171.
 - [17] E. Witten, Nucl. Phys. **B160**, 57 (1979).
 - [18] J. M. Maldacena, Adv. Theor. Math. Phys. **2**, 231 (1998).
 - [19] J. B. Kogut, D. K. Sinclair, S. J. Hands, and S. E. Morrison, Phys. Rev. **D64**, 094505 (2001), hep-lat/0105026.
 - [20] P. Giudice and A. Papa, Phys. Rev. D **69**, 094509 (2004), hep-lat/0401024.
 - [21] P. Cea, L. Cosmai, M. D'Elia, and A. Papa, JHEP **0702**, 066 (2007), hep-lat/0612018.
 - [22] P. Cea, L. Cosmai, M. D'Elia, and A. Papa, PoSLAT2007 p. 214 (2007), 0710.2068.
 - [23] P. Cea, L. Cosmai, M. D'Elia, and A. Papa, Phys. Rev. D **77**, 051501 (2008), 0712.3755.
 - [24] P. Cea, L. Cosmai, M. D'Elia, and A. Papa, Nucl. Phys. **A820**, 239c (2009), 0812.2777.
 - [25] P. Cea, L. Cosmai, M. D'Elia, C. Manneschi, and A. Papa, Phys. Rev. D **80**, 034501 (2009), 0905.1292.
 - [26] W. Pauli, Nuovo Cimento **6**, 205 (1957).
 - [27] W. Pauli, *ibid* **7**, 411 (1958).
 - [28] T. Brauner, K. Fukushima, and Y. Hidaka, Phys. Rev. D **80**, 074035 (2009), 0907.4905.
 - [29] D. Blaschke, M. Buballa, A. E. Radzhabov, and M. K.

- Volkov, Phys. Atom. Nucl. **71**, 2008 (2008), 0705.0384.
- [30] G. A. Contrera, D. Gomez Dumm, and N. N. Scoccola, Phys. Atom. Nucl. **Phys.Lett.B661**, 2008 (2008), 0711.0139.
- [31] K.-I. Kondo, Phys. Rev. D **82**, 065024 (2010), 1005.0314.
- [32] T. Hell, K. Kashiwa, and W. Weise, Phys. Rev. D **83**, 114008 (2011), 1104.0572.
- [33] V. Pagura, D. Gomez Dumm, and N. N. Scoccola (2011), 1105.1739.
- [34] K. Morita, V. Skokov, B. Friman, and K. Redlich, Phys.Rev. **D84**, 076009 (2011), 1107.2273.
- [35] K. Fukushima and K. Kashiwa (2012), 1206.0685.
- [36] A. Barducci, R. Casalbuoni, G. Pettini, and R. Gatto, Phys. Lett. **B301**, 95 (1993), hep-ph/9212276.
- [37] K. Kashiwa, M. Yahiro, H. Kouno, M. Matsuzaki, and Y. Sakai, J. Phys. **G36**, 105001 (2009), 0804.3557.
- [38] K. Kashiwa, H. Kouno, T. Sakaguchi, M. Matsuzaki, and M. Yahiro, Phys. Lett. **B647**, 446 (2007), 0608078.